Linear Barotropic Simulation of Atmospheric Low-Frequency Variability

Werner Metz

Abstract

A steady-state barotropic model, linearized about a GCM-derived 500 hPa basic state, is driven by a sample of "observed" forcing fields. It turns out that the leading mode (LEOF) obtained from the sample of linear solutions matches well with the leading EOF of low-frequency atmospheric variability actually occurring in the GCM. The response of the linear model is analysed in terms of the singular modes of the model's linear operator. It is found that about 50 percent of the spatial variance of the LEOF can be explained in terms of the leading two singular modes. This finding is reflected also in the linear barotropic energy balance of the LEOF which shows that the mode is maintained through nearly equal contributions from i) the kinetic energy conversion of basic state kinetic energy (which is primarily due to the action of the singular modes) and ii) the forcing. The linear simulation of the GCM EOF fails if the linear model is linearized about a 300 hPa basic. This is explained by the fact that in this case the structure of the leading singular modes, which have a strong impact on the linear response, is much more dissimilar to the structure of the GCM EOF than in the 500 hPa case.

Zusammenfassung

Ein stationäres barotropes Modell, das bezüglich eines (aus einem GCM Experiment abgeleiteten) 500 hPa Grundzustandes linearisiert ist, wird für einen Satz von "beobachteten" Antriebsfeldern gelöst. Dabei zeigt sich, daß die führende Mode der langperiodischen atmosphärischen Variabilität (EOF) im GCM Experiment durch das lineare Modell sehr gut simuliert wird. Weiterhin stellt sich heraus, daß hierfür die Antriebsfelder und die singulären Moden des linearen Modelloperators die gleiche Bedeutung besitzen. Auf die Wichtigkeit der Anwendung des Modells bezüglich des äquivalent-barotropen Niveaus wird hingewiesen.

1. Introduction

It is well known that the atmospheric low-frequency variability (at time scales greater than two weeks, say) is characterized by the existence of recurring, spatially organized and geographically fixed flow patterns and that only a handful of such patterns explain the by far largest part of the total variance of the atmospheric flow. In recent years, a number of possible mechanisms for the excitation and/or maintenance of these modes have been put forward, however, in this short note we are concerned only with internal dynamical mechanisms that rely on the barotropic energy transformation from the standing wave field to the low-frequency modes.

In an illuminating study Branstator (1990) forced a stationary linearized version of a GCM (with a wavy basic state) with a large sample of random forcing fields. When computing the (streamfunction) EOFs of these forced solutions he found that some of these EOFs were similar to the EOFs of the monthly mean fields as obtained from the original, nonlinear climate mode GCM run. He concluded that "*the geographical distribution of low-frequency variability is likely to occur chiefly as a result of influences of the large-scale stationary*

waves. Spatially organized external forcing anomalies are not necessary to explain the preference of the atmosphere for these patterns".

These conclusions were supported by Navarra (1993) who showed that the EOFs of a white noise forced linear stationary model are the Schmidt modes (called "singular modes" in the following) which can be obtained from a singular value decomposition (SVD) of the model's linear operator. Starting from the linearized barotropic vorticity equation, he examined the singular modes of an observed 300 hPa basic state (with the standing waves included) and found that the most important modes exhibited a characteristic teleconnection structure if an appropriate linear friction was used.

Following along these lines, Metz (1994, M94 in the following) investigated the sensitivity of these barotropic singular modes to changes in the basic state and found (using GCM derived data) that the pattern of the most important singular mode matches most favourably to the pattern of the leading low-frequency mode actually occurring in the GCM if an equivalent-barotropic basic state is used.

On the other hand, there is ample evidence (e.g. Lau 1988, Metz 1991, Branstator 1992) that the forcing (in terms of the barotropic vorticity equation) that is actually associated with observed or GCM-simulated low-frequency modes is highly organized and thus far from being white noise. That means, that for an "observed" forcing the exact association between the singular modes and the EOFs of the linear forced solutions breaks down. Nevertheless, the singular modes are excited also under such circumstances and it has been shown by M94 that a few of these modes provide a major contribution to the EOFs of linear forced solutions with a 300 hPa basic state. Unfortunately, in this case with the 300 hPa basic state, the most important singular modes were not similar to the actual GCM-EOFs and thus, the importance of the singular modes for the GCM low-frequency variability could not be established.

The purpose of the present note is to repeat the experiments of M94, but using an *equivalent-barotropic* basic state and the associated *equivalent-barotropic* forcing with the linear barotropic vorticity equation. As mentioned above, in this case the coincidence between the patterns of the leading singular mode and the leading actual GCM-EOF is much better, and thus, it will be interesting to examine the role of the singular modes under such circumstances.

The paper is organized as follows. The GCM experiment considered and the low-frequency variability simulated in this experiment is briefly discussed in section 2. In section 3, we describe the experiments with the linear forced model, where the 500 hPa level is used to approximate the equivalent-barotropic level, and the EOFs of the linear model solutions are evaluated. The leading EOF1 obtained from these experiments is then analysed in terms of the singular modes in section 4. A summary and conclusions are given in section 5.

2. Low-frequency variability in the GCM

Following M94 we investigate the variability in a GCM as a substitute for the observed atmospheric variability. This proceeding has the advantage that a large sample of dynamically

consistent data will be available for the analysis. The particular GCM experiment we consider is a 20 years integration (Roeckner et al. 1992) of the Hamburg version of the ECMWF T21 spectral model, performed to simulate present climate conditions. The effects of low-frequency variations of the boundary conditions are represented in terms of monthly varying, prescribed sea-surface temperatures (SSTs). From this GCM experiment we have retrieved daily global fields of vorticity and divergence at standard pressure levels in the form of complex spherical harmonics coefficients. Only the last 18 winters (DJF) of the experiments were analysed.

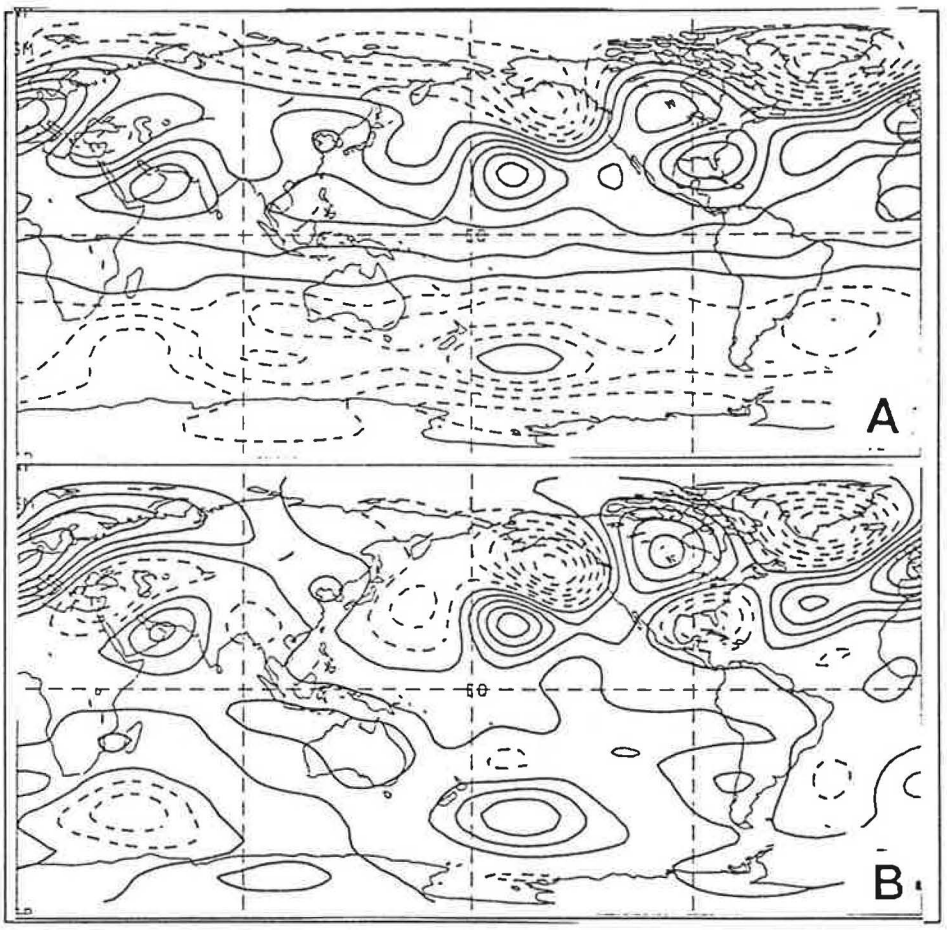

FIG. 1. The leading EOF1 of intraseasonal wintertime equivalent-barotropic vorticity variability for the GCM experiment. (a) The total streamfunction ($\nabla^{-2}\xi$) and (b) the eddy (m>0) streamfunction. Contour interval arbitrary, but identical for (a) and (b). Negative contours dashed. Redrawn from Metz (1994).

The low-frequency intraseasonal atmospheric variability of this GCM-experiment has been evaluated in M94 in terms of a principal component analysis of monthly mean fields (with the interannual variability removed) of the equivalent-barotropic relative vorticity ξ_{eq} (for definition cf. M94). The leading eigenmode of this principal component analysis explains 13.7 percent of the intraseasonal vorticity variance of the monthly mean GCM flow and has been associated by M94 with a distinct dynamical mode. The pattern (in terms of streamfunction) of the associated eigenvector[1] is displayed for convenience in Fig. 1a and the

[1]Performing the principal component analysis on streamfunction gives little change in the pattern structure but the first EOF explains now 39.2 percent of variance.

eddy pattern (m>0) in Fig. 1b. Please note that the Pacific-North American component of the eddy pattern is very reminiscent of the well-known PNA teleconnection of Wallace and Gutzler (1981). We shall consider these patterns (EOF1 in what follows) as a verification standard for the linear model experiments to be described in what follows.

3. A linear forced model

In this section we want to simulate the patterns of Fig. 1 using a linear model driven by a sample of GCM derived forcing fields and to evaluate then the EOFs of the resulting sample of linear solutions. In M94, it has been shown that the success of such a simulation depends strongly on the proper choice of the basic state (and, of course on the dissipation constants) and it has been suggested that an equivalent-barotropic basic state should be most appropriate for that purpose. In particular, this suggestion was based on the finding that the leading singular mode (to be defined in the next section) was much more similar to the EOF1 of the GCM experiment when the basic state was equivalent-barotropic than when it was evaluated at 300 hPa.

a. Model description

Our model is based on the linearized, steady-state vorticity equation. Decomposing all variables are into a basic state, a low-frequency (quasi-stationary) perturbation and a high-frequency deviation thereof, i.e.:

$$\xi = \xi_b + \tilde{\xi} + \xi', \quad \text{where } \widetilde{(\xi')} = 0 \tag{1}$$

and assuming stationarity for the low-frequency components, the linearized steady-state perturbation equation for the low-frequency components reads:

$$\nabla \cdot \tilde{v}(\xi_b + f) + \nabla \cdot v_b \tilde{\xi} + \alpha \tilde{\xi} + \gamma \nabla^4 \tilde{\xi} = -\nabla \cdot \widetilde{v'\xi'} - \nabla \cdot f\tilde{v}_\chi . \tag{2}$$

Here, $v = k \times \nabla\psi$ is always the rotational wind while v_χ represents the divergent wind. In deriving (2) the vertical advection and twisting terms and the vorticity transport by the high-frequency *divergent* transients have been neglected and in the last term on the rhs the absolute vorticity has been replaced by f. Linear (Ekman) friction and biharmonic diffusion terms have been routinely added. Making the equivalent-barotropic assumption for the basic state and the low-frequency components and averaging (2) in the vertical yields the equivalent-barotropic version of (2). Associating $v_b, \tilde{v}, \xi_b$ and $\tilde{\xi}$ with their equivalent barotropic values, (2) can be solved for $\tilde{\xi}$ provided the rhs:

$$\tilde{F} = -\frac{\kappa}{p_0} \int_0^{p_0} \left[\nabla \cdot \widetilde{v'\xi'} + \nabla \cdot f\tilde{v}_\chi \right] dp \tag{3}$$

is prescribed as a forcing term. In (3), κ is an empirical constant. The linear equation (2) with the rhs given by (3) should be applied at the equivalent-barotropic level. We approximate this

level by the *500 hPa* level. Furthermore, the forcing (3) is approximated by evaluating the integrand at the *500 hPa* level, too.

b. Variability in the linear model

The basic state v_b, ξ_b is evaluated using the (18 winter) mean 500 hPa vorticity of the GCM experiment and the forcing (3) is computed using daily 500 hPa data for each of the (54) winter months. Guided by the results of M94 we set the dissipation parameters in (2) as $1/\alpha$ =5.0 days and γ=2.0 $10^{16}m^4s^{-1}$. Using these 54 forcing fields the linear model is solved for a global domain on the sphere yielding a sample of 54 linear vorticity solutions. The dominant modes of variability of this sample are then evaluated in terms of a principal component analysis of the associated vorticity covariance matrix. To avoid confusion with the EOFs of the original GCM experiment, the eigenvectors obtained from the linear solutions are termed "LEOFs".

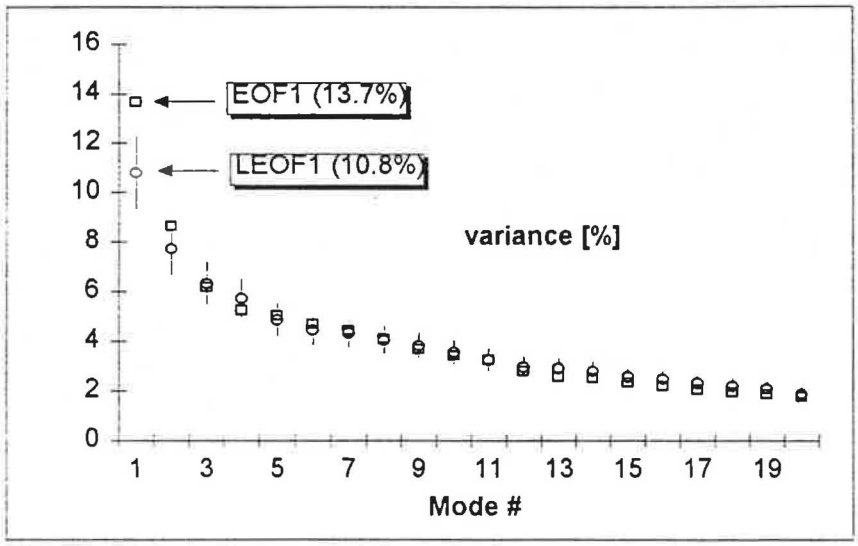

FIG. 2. The LEOF eigenvalue spectrum (only the 20 largest eigenvalues) and associated sample error bars (54 dofs). Also shown (open squares) are the eigenvalues obtained from the GCM experiment.

The LEOF eigenvalue spectrum obtained is displayed in Fig. 2. The LEOF1 explains 10.8 percent of the intraseasonal vorticity variance of the sample of forced solutions and the sampling error bars suggest that it can be associated with a distinct dynamical mode, too. Also shown in Fig. 2 is the EOF eigenvalue spectrum as obtained by M94 for the GCM experiment. The shapes of the two spectra are generally similar, however, the eigenvalue associated with EOF1 is larger than those associated with LEOF1. Leaving sampling effects out of consideration, this indicates (as one should expect) that the linear forced model represents only part of the physical mechanisms which co-operate to constitute the pronounced EOF1 mode in the GCM experiment.

The (streamfunction) pattern that is associated with the LEOF1 is illustrated in Fig. 3. It is evident that the linear model does a good job in recovering nearly every detail of the arching PNA-like main component of the EOF1. Outside of this component, particularly over the Atlantic-European sector, there is little similarity which leads to a correlation of 0.438 in terms of global vorticity between the two patterns of Fig. 1a and 3a.

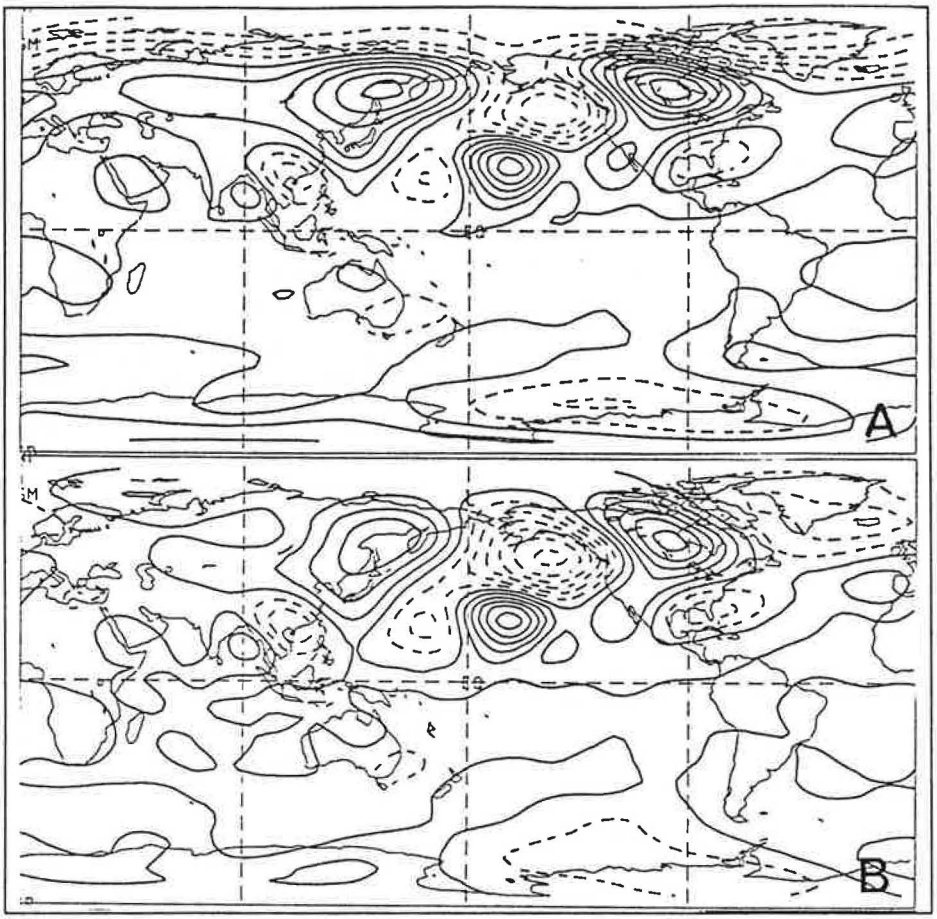

FIG. 3. As Fig. 1 but for the leading LEOF1 of the linear forced model.

c. Energetics

The (steady-state) kinetic energy balance for a LEOF may be written symbolically as

$$Ck_n + D_n + S_n = 0 \tag{4a}$$

where

$$\begin{aligned} \tilde{K}_n &= -\left\langle \tilde{\psi}_n \tilde{\xi}_n \right\rangle \\ Ck_n &= C(K_b, \tilde{K}_n) = \left\langle \tilde{\psi}_n [\nabla \cdot \tilde{v}_n (\xi_b + f) + \nabla \cdot v_b \tilde{\xi}_n] \right\rangle \\ D_n &= \left\langle \tilde{\psi}_n (\alpha + \gamma \nabla^4) \tilde{\xi}_n \right\rangle \\ S_n &= -\left\langle \tilde{\psi}_n \tilde{F}_n \right\rangle \end{aligned} \tag{4b}$$

are the kinetic energy of LEOFn, the kinetic energy conversion from the basic state to the LEOFn, the dissipation and the energy source due to the forcing. In (4b), $\tilde{\psi}_n$ and $\tilde{\xi}_n$ denote the streamfunction and vorticity of an LEOFn and $\tilde{F}_n$ the associated forcing (computed as an residuum, cf. M94). The angle brackets represent a spatial mean over the whole globe.

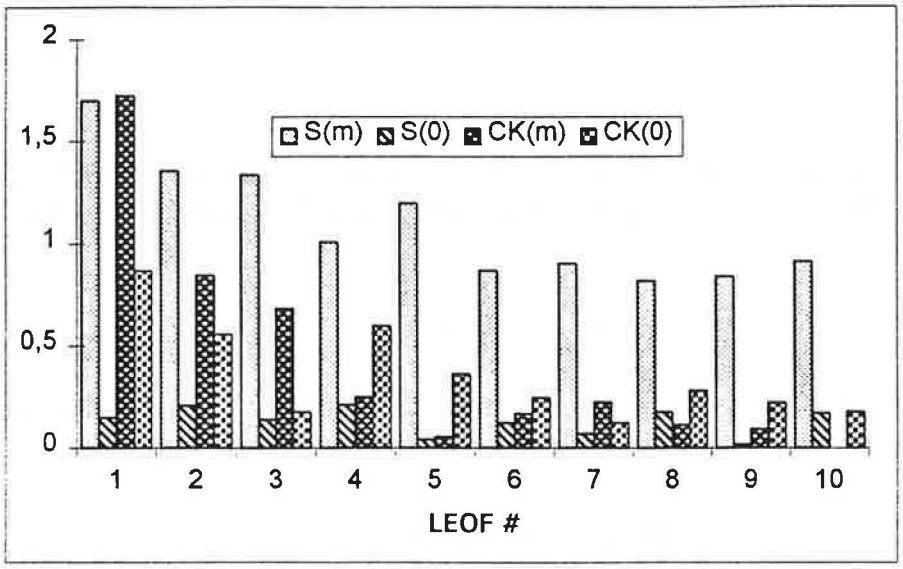

FIG. 4. The kinetic energy conversion Ck_n and the forcing energy source S_n as computed for the 10 leading LEOFs. Both terms are broken into their zonal mean (m = 0) and eddy (m > 0) components. Units are 10^{-2} W/m^2.

The kinetic energy conversion Ck_n and the energy source S_n are displayed in Fig. 4 for the first 10 LEOFs, where both terms were broken into their zonal mean (m = 0) and eddy (m > 0) parts. One finds that for LEOF1 Ck_n(m>0) and S_n(m>0) are of the same magnitude and that the mode as a whole is dominated by an energy gain via Ck_n. This contribution via of Ck_n decreases with increasing mode number, making the energy source due to the forcing the dominating term already beyond LEOF2. The dissipation D_n (not shown) balances the sum of Ck_n and S_n. Thus, the energy supply from the basic state into the LEOFs is confined to a few leading LEOFs and we shall demonstrate in what follows that this mechanism is mainly realized in terms of a few singular modes.

4. Analysis of the LEOFs in terms of singular modes

It was shown in M94 that the LEOFs associated with the sample of solutions of a linear forced model are strongly affected by the mathematical properties of the model's linear operator, which are manifested in terms of its right and left singular vectors. In M94 these singular vectors severely downgraded the skill of the forced linear model to simulate the main variability mode (EOF1) of the GCM experiment, when a 300 hPa basic state was used for the linearization of the model. In this section we want to evaluate the influence of these singular vectors on the LEOFs as obtained in the previous section, for a 500 hPa basic state.

a. Mathematics

After discretization (in terms of spherical harmonics) of the linear vorticity equation (2) the resulting coupled system of inhomogeneous equations may be written in matrix form as:

$$\boldsymbol{A}\boldsymbol{x} = \boldsymbol{f}, \tag{5}$$

where $\boldsymbol{A}$ is the (real) system matrix[2] which is in general quadratic but not symmetric, $\boldsymbol{x}$ the state vector (representing vorticity) and $\boldsymbol{f}$ the corresponding state vector for the forcing. The singular value decomposition (SVD) of $\boldsymbol{A}$ is:

$$\boldsymbol{A} = \boldsymbol{U}\,\Sigma\,\boldsymbol{V}^T, \tag{6}$$

where U and V are orthogonal matrices, the columns of which are called the *left* and *right singular vectors*, and Σ is the diagonal matrix of the singular values σ_k. Using (6), (5) may be solved for $\boldsymbol{x}$ to yield:

$$\boldsymbol{x} = \boldsymbol{V}\,\Sigma^{-1}\;\boldsymbol{U}^T\boldsymbol{f}. \tag{7}$$

Thereby it is assumed that all singular value σ_k are non-zero, i.e. that the matrix $\boldsymbol{A}$ is *not* singular. Expanding the matrix multiplication in (7) yields an alternate form:

$$\boldsymbol{x} = \sum_k \boldsymbol{v}_k \sigma_k^{-1}\left(\boldsymbol{u}_k^T\boldsymbol{f}\right), \tag{8}$$

where k runs from 1 to n and n being the number of columns (rows) of $\boldsymbol{A}$ (n = 483 for the truncation T21 used throughout in this study). (8) is the key equation for our problem which describes the impact of the right singular vectors on a linear forced solution $\boldsymbol{x}$. It shows that some right singular vector $\boldsymbol{v}_k$ makes a large contribution to $\boldsymbol{x}$, if i) the associated *singular value* σ_k is *small* and ii) the *scalar product* (inner product) between the associated *left singular vector* $\boldsymbol{u}_k$ and the forcing $\boldsymbol{f}$ is *large*. The pair of left and right singular vectors $(\boldsymbol{u}_k, \boldsymbol{v}_k)$ together with the associated singular value σ_k constitute a *singular mode*.

b. Singular modes

The SVD of the matrix $\boldsymbol{A}$ for the present 500 hPa basic state and the present setting of the dissipation parameters has been performed by M94. The matrix condition number $OND = \sigma_{min}/\sigma_{max}$ which measures the "singularity" of $\boldsymbol{A}$ is 7.8×10^{-3} and thus of the same order than that obtained by M94 for the 300 hPa basic state.

---

[2]In the following formulas bold uppercase italics denote matrices and bold lowercase italics denote vectors.

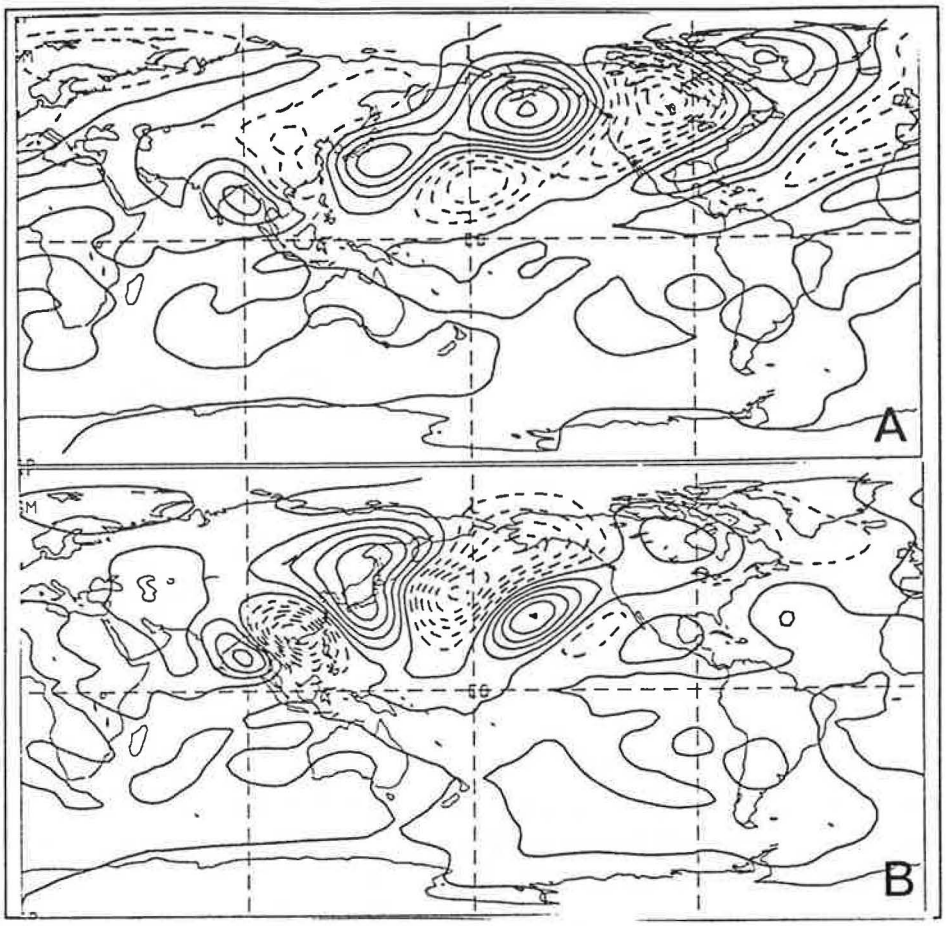

FIG. 5. The (streamfunction) patterns associated with the leading two right singular vectors. (a) Right singular vector v_1 and (b) right singular vector v_2. Only the eddy components of the patterns are shown. Contour interval arbitrary.

As it is clear from (8) that those singular modes with the smallest singular values are potentially most easily excited, we display in Fig. 5 the (streamfunction) patterns of the two right singular vectors with the two smallest singular values, i.e. v_1 and v_2. The total streamfunction (not shown) has a large zonal mean component (similar to that of M94, Fig. 12a) but the eddy component of v_1 (Fig. 5a) exhibits a certain similarity with both the eddy structure of the LEOF1 (Fig. 3b) and that of the GCM experiment EOF1 (Fig. 1b). The eddy pattern of v_2, on the other hand, consists of an arching wave train over the Central and West Pacific and does not resemble the EOF1.

The contribution that each singular mode makes to the pattern of the LEOF1 can be easily computed on the basis of (8). As

$$\left(v_k^T x\right) = \left(v_k^T v_k\right)\sigma_k^{-1}\left(u_k^T f\right) \tag{9}$$

due to the orthogonality of the v_k's, an explicit knowledge of the forcing associated with an LEOF is *not* necessary to evaluate the degree to which each right singular vector is excited.

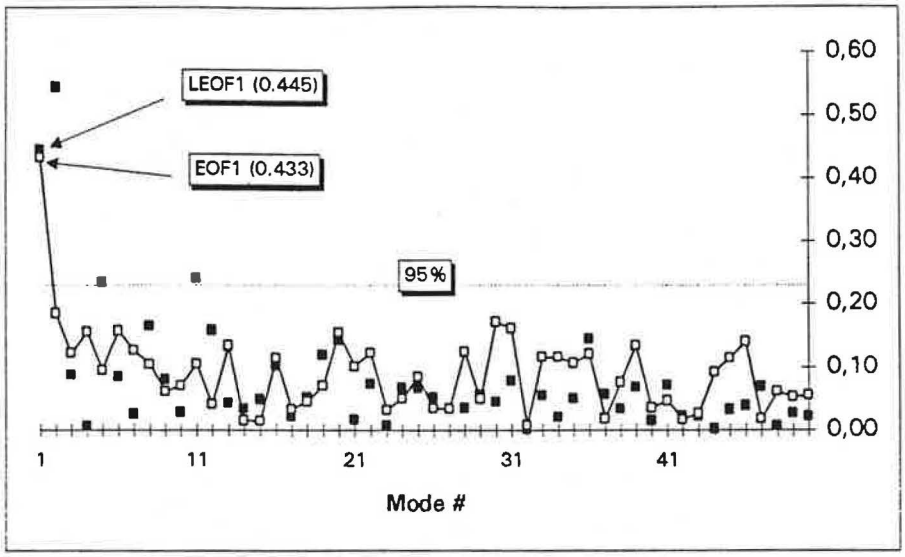

FIG. 6. The pattern correlation between the LEOF1 and the 50 leading right singular vectors (bold squares). Also shown (open squares) is the pattern correlation between the GCM experiment EOF1 and the singular vectors. The 95 percent significance limit for the pattern correlations is based on 70 *dofs*.

The pattern correlation (i.e. the *lhs* of (9) normalized by the corresponding spatial standard deviations) between the LEOF1 and the leading 50 right singular vectors is illustrated in Fig. 6. One can see that only the first two singular modes contribute significantly to the LEOF1. Taken together, these first two singular modes are able to explain about 50 percent of the spatial variance (in terms of global vorticity) of the LEOF1. By inspecting the patterns of the singular vectors (Fig. 5a,b) on recognizes that the action of $\boldsymbol{v}_2$ is to get the right position of the East-Pacific high-low dipole component of the LEOF1 pattern. Also shown in Fig. 6 is the pattern correlation between the right singular vectors and the EOF1 of the GCM experiment. The only significant correlation (0.433) is associated with $\boldsymbol{v}_1$ which means that about 19 percent of the EOF1 vorticity variance[3] can be explained by the linear mode.

Let us now examine how the excitation of the leading two singular modes takes place. For that purpose, we show in Fig. 7 the patterns of the two *left* singular vectors $\boldsymbol{u}_1$ and $\boldsymbol{u}_2$. As discussed above, these patterns represent the (vorticity) forcings that optimally excite the respective right singular vectors. One finds, that $\boldsymbol{u}_1$ consists basically of two components, a strong large-scale pattern with an E-W dipole at high latitudes and a weaker small-scale wave train at tropical to subtropical latitudes over the south-east coast of Asia. The same components occur also for $\boldsymbol{u}_2$ but their relative magnitudes are reversed. Thus, one may speculate that the leading right singular vector $\boldsymbol{v}_1$ can be preferably exited by a high-latitude vorticity forcing, while the right singular vector $\boldsymbol{v}_2$ is preferably exited by a tropical or subtropical vorticity forcing. To verify this speculation, we display in Fig. 8 the spatial structure of the forcing $\tilde{F}_1$ that is associated with the LEOF1. One can see, that this forcing pattern consists primarily of two wave trains. One is extending from the subtropical Central-Pacific towards Alaska having its largest amplitudes at high latitudes. This forcing component should be able to excite $\boldsymbol{v}_1$. The other component extends along the south-east Asian coast and can thus excite $\boldsymbol{v}_2$. Moreover, we have verified that it are just these two regions where the 500

[3]Note, however, that these figures refer to global vorticity. If one compares the patterns in terms of eddy streamfunction the corresponding figures are 0.677 and 46 percent (cf. M94, Tab. 6)

hPa forcing exhibit local maxima of its intraseasonal standard deviation (not shown), and this explains the occurrence of the LEOF1 in the linear model.

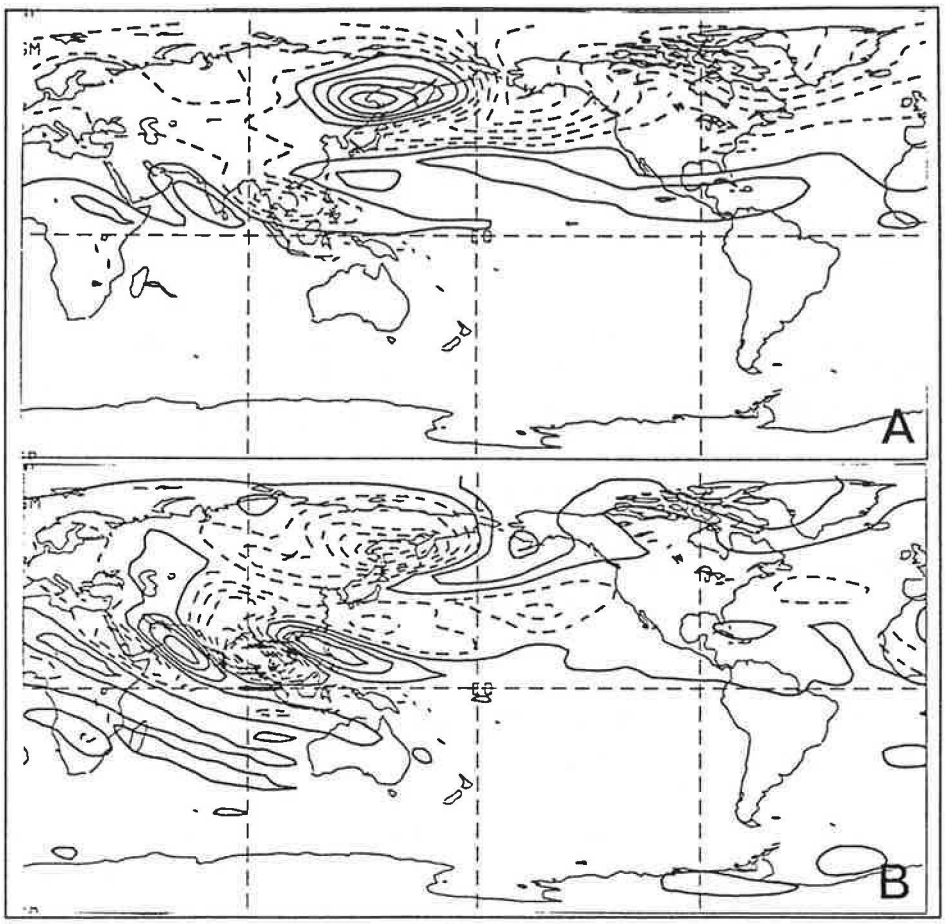

FIG. 7. The patterns (corresponding to a vorticity tendency) of the leading two left singular vectors. (a) Left singular vector u_1 and (b) left singular vector u_2. Shown is the total pattern. Contour interval arbitrary.

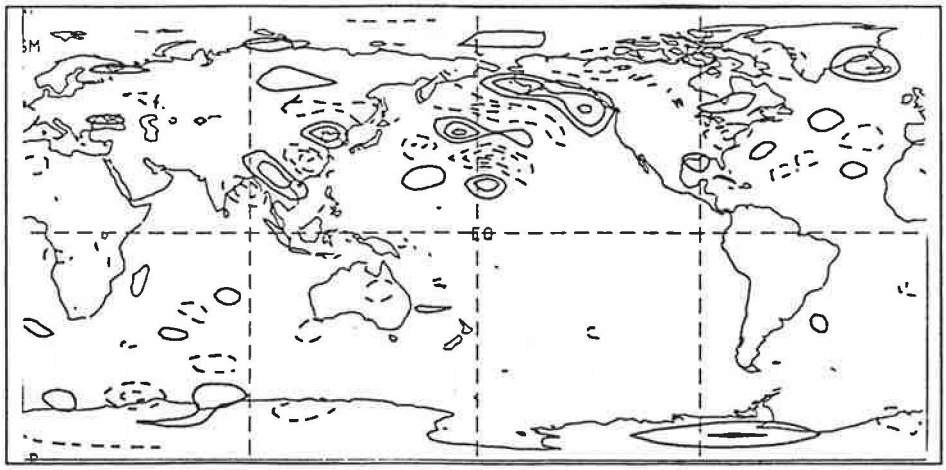

FIG. 8. The vorticity forcing pattern f_1 (corresponding to a vorticity tendency) associated with the LEOF1 of Fig. 3a. Contour interval arbitrary.

5. Summary and conclusions

The results described above show that the leading mode (EOF1) of the intraseasonal low-frequency atmospheric variability (of a GCM experiment) is well simulated by the leading EOF (LEOF1) obtained from a sample of linear forced solutions of a steady-state barotropic model if both, the basic state and the vorticity forcing are derived under the equivalent-barotropic assumption (approximated by the 500 hPa level). On the other hand, it has been shown by M94 that this is not possible it the basic state and the vorticity forcing are derived using the 300 hPa level, instead.

This sensitivity of the skill of the linear model is attributed to the mathematical properties of the model's linear operator which are described in terms of its singular modes. In fact, for a reasonable values of the dissipation parameters, it is shown (in the present study and in M94) that the LEOF1 of the linear model solutions is always significantly influenced by a few of these singular modes. For example, about 50 (60) percent of the spatial vorticity variance of the LEOF1 can be explained by the first two (the first) right singular vectors for the 500 hPa (300 hPa) basic state. Thus, the success or failure of the linear model is likely related to the similarity or dissimilarity of the leading singular modes with the pattern to be simulated, i.e. the EOF1.

In a more physical context, the singular modes represent the way[4] how the barotropic kinetic energy conversion from the basic into the quasi-stationary perturbations (i.e. Ck_n) is realized in the linear model and it is shown above (Fig. 4) that about 50 percent of the total kinetic energy input into the eddy component of the LEOF1 comes from this conversion. This finding agrees with results of other studies (e.g. Nakamura et al. 1987 or Branstator 1992) of the energy balance of observed low-frequency modes.

On the other hand, the other 50 percent of the energy input come from the forcing which means that in the linear model the two mechanisms are equally important. This suggests that the choice of an equivalent-barotropic basic state *alone* is not sufficient to guarantee the success of the linear model simulation (with a realistic, i.e. non-white noise forcing) but that this success is due to a delicate interplay between the forcing and the singular modes. This suggestion has been verified by repeating the experiment as described in section 3b using the same dissipation parameters but i) a 300 hPa basic state with the 500 hPa forcing (3) and ii) a 500 hPa basic state and the 300 hPa forcing of M94. In neither of these experiments the resulting LEOF1 (not shown) exhibited any significant pattern correlation with the GCM EOF1.

Finally, let us comment in the relevance of the linear singular modes for the excitation of the EOF1 in the nonlinear GCM experiment (or in the real atmosphere). It is clear that in the GCM experiment a number of additional mechanisms are acting. These include, for example, the low-frequency variability of boundary conditions (SST), baroclinic effects, nonlinearity and transience. Thus it is unlikely that one mechanism alone is responsible for the occurrence of the EOF1 but that some (or many) mechanisms are acting together. Nevertheless, as we have shown, the leading singular mode of the linear model projects significantly onto the

---

[4]Note, however, that by definition the singular modes represent not only the linear interaction between the basic state and the steady-state perturbation, but include also the dissipation effects.

EOF1 and explains about 19 percent of its spatial (vorticity) variance. This indicates that the linear mechanism discussed in this paper must be considered as an important factor acting in the nonlinear and transient GCM flow, too. Lastly, this finding emphasizes once more the necessity of a precise simulation of the standing wave field to obtain a correct simulation of the atmospheric low-frequency variability.

Acknowledgments

The assistance of Drs. Uwe Harlander and Yorck von Detten of the Meteorologisches Institut der Universität München in processing some of the figures is gratefully acknowledged.

References

Branstator, G.,1990: Low-frequency patterns induced by stationary waves. *J. Atmos. Sci.*, **47**, 629-648.

Branstator, G.,1992: The maintenance of low-frequency anomalies. *J. Atmos. Sci.*, **48**, 1924-1945.

Lau, N.-C., 1988: Variability of the observed midlatitude storm tracks in relation to low-frequency changes in the circulation patterns. *J. Atmos. Sci.*, **45**, 2718-2743.

Metz, W., 1991: Optimal relationship of large-scale flow patterns and the barotropic feedback due to high-frequency eddies. *J. Atmos. Sci.*, **48**, 1141-1159.

Metz, W., 1994: Singular modes and low-frequency atmospheric variability. *J. Atmos. Sci.*, **51**, 1740-1753.

Nakamura, H., M. Tanaka, and J.M. Wallace, 1987: Horizontal structure and energetics of northern hemisphere wintertime teleconnection patterns. *J.Atmos.Sci.*, **44**,3377-3391.

Navarra, A., 1993: A new set of orthogonal modes for linearized meteorological problems. *J. Atmos. Sci.*, **50**, 2569-2583.

Roeckner, E., K. Arpe, L. Bengston, S. Brinkop, L. Dümenil, M. Esch, E. Kirk, F. Lunkeit, M. Ponater, B. Rockel, R. Sausen, U. Schlese, S. Schubert and M. Windelband, 1992: Simulation of the present-day climate with the ECHAM model: Impact of model physics and resolution. Rept. no. 93, Max-Planck-Institut für Meteorologie, Hamburg, 172 pp., available on request.

Wallace, J.M. and D.S. Gutzler, 1981: Teleconnections in the geopotential height field during the Northern Hemisphere winter. *Mon. Wea. Rev.*, **109**, 785-812.